

Surface-Patterned DNA Origami Rulers Reveal Nanoscale Distance Dependency of the Epidermal Growth Factor Receptor Activation

Ivy Mayer, Tina Karimian, Klavdiya Gordiyenko, Alessandro Angelin, Ravi Kumar, Michael Hirtz, Ralf Mikut, Markus Reischl, Johannes Stegmaier, Lu Zhou, Rui Ma, Gerd Ulrich Nienhaus, Kersten S. Rabe, Peter Lanzerstorfer, Carmen M. Domínguez,* and Christof M. Niemeyer*



Cite This: <https://doi.org/10.1021/acs.nanolett.3c04272>



Read Online

ACCESS |

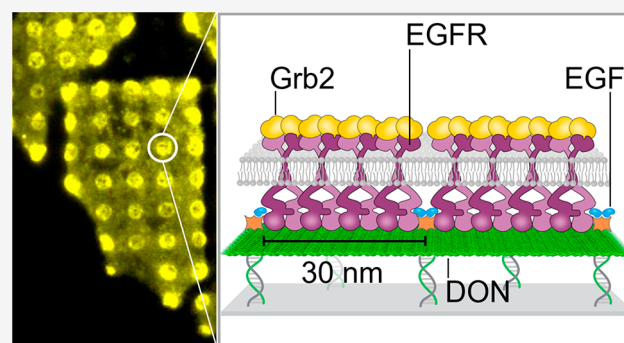
Metrics & More

Article Recommendations

Supporting Information

ABSTRACT: The nanoscale arrangement of ligands can have a major effect on the activation of membrane receptor proteins and thus cellular communication mechanisms. Here we report on the technological development and use of tailored DNA origami-based molecular rulers to fabricate “Multiscale Origami Structures As Interface for Cells” (MOSAIC), to enable the systematic investigation of the effect of the nanoscale spacing of epidermal growth factor (EGF) ligands on the activation of the EGF receptor (EGFR). MOSAIC-based analyses revealed that EGF distances of about 30–40 nm led to the highest response in EGFR activation of adherent MCF7 and Hela cells. Our study emphasizes the significance of DNA-based platforms for the detailed investigation of the molecular mechanisms of cellular signaling cascades.

KEYWORDS: DNA nanostructures, cell signaling, epidermal growth factor receptor, self-assembly, surfaces, subcellular micropatterning



The study of cellular communication mechanisms is of utmost importance for both basic and applied research in the biomedical sciences. Key elements in the interaction of cells with their environment are membrane receptor proteins. Upon binding their cognate ligands, receptors initiate a cascade of signaling events inside the cell, which ultimately triggers a biological response. Frequently, the access of ligands to receptors is geometrically constrained, be they proteins presented by neighboring cells, such as ephrins, or soluble ligands, such as growth factors presented by the extracellular matrix.^{1–3} Although this phenomenon has been observed in several systems, such as the epidermal growth factor (EGF) receptor (EGFR),⁴ ephrin receptors (Ephs),⁵ and “immunological synapses” in B- and T-cells,⁶ the detailed study of the spatial receptor organization remains a great challenge due to its dynamic and transient nature. A promising approach to overcome these problems takes advantage of perturbation analyses based on membrane proteins in living cells interacting with surface-immobilized ligand patterns. The effect on signaling of geometrically constrained ligands presented by these surfaces can then be analyzed by microscopy.^{3,7} This approach would benefit from patterning techniques, which enable precise arrangement of ligand assemblies with full control over the absolute number, stoichiometry, and nanoscale orientation.⁸ The Spatz group has shown early on that some of these limitations can be overcome by combining “top-down” and “bottom-up” self-assembly with the so-called “block

copolymer micelle nanolithography”, which has enabled quantitative studies on the nanoscale distance dependence of the activation of integrin transmembrane receptors.^{9,10} However, even this approach does not offer the possibility of arranging different numbers of ligands with molecular resolution.

Because DNA origami nanostructures (DON) can be easily and efficiently modified with proteins and other components at near molecular resolution,¹¹ they are increasingly proving to be a powerful tool for studying biological processes such as cell adhesion and activation.^{12–28} Our group has developed the so-called “Multiscale Origami Structures As Interface for Cells” (MOSAIC) technique¹³ to overcome the problems of alternative techniques described above. MOSAIC takes advantage of top-down printed DNA patterns of $\sim 5 \mu\text{m}$ spots, i.e., with subcellular dimensions, which are used for the DNA-directed immobilization (DDI) of double-sided functionalized DONs carrying anchor strands and ligand patterns on the bottom and top side, respectively, of a quasi-two-

Received: November 6, 2023

Revised: December 21, 2023

Accepted: December 22, 2023

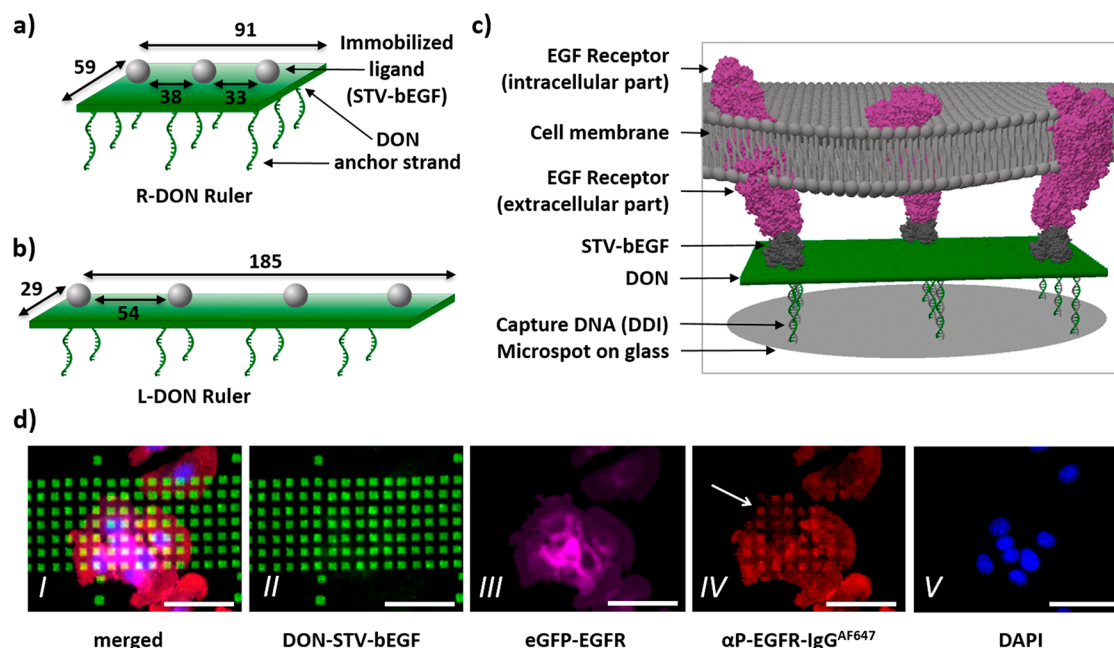


Figure 1. Working principle of MOSAIC. (a, b) Schematic representation of ligands arranged on rectangular and longitudinally elongated DNA origami nanostructures (R-DON, and L-DON, respectively) with variable distances (given in nanometers) to investigate distance-dependent activation of the receptors. (c) After immobilization of the DON rulers through the protruding anchor strands on DNA microspots, their interaction with membrane receptors can be analyzed. (d) Representative fluorescence micrographs ($340 \times 250 \mu\text{m}^2$) from cell experiments. The ligand-decorated DONs were immobilized on DNA microarrays, leading to spot patterns with a lateral extension of $\sim 5 \mu\text{m}$ shown in panel II (green). MCF7 cells expressing an eGFP-tagged EGF receptor (eGFP-EGFR) were allowed to adhere to the obtained chips (magenta, panel III). After fixation and immunostaining, signals from activated eGFP-EGFR are visible as red spots through a specific antibody ($\alpha\text{P-EGFR-IgG}^{\text{AF647}}$, marked by a white arrow in panel IV). Cell nuclei are visualized by DAPI staining (blue, in panel V). Panel I shows a merged picture of all panels (II–V). Scale bars: $50 \mu\text{m}$.

dimensional rectangular scaffold plate (Figure 1a,b). Subsequent to DDI, the micro-/nanopatterned surface can be used for cell adhesion (Figure 1c), and activated receptors can be detected by either live-cell imaging or immunostaining (Figure 1d). Because our pioneering work suggested a dependence of EGFR activation on the nanoscale arrangement of EGF ligands,¹³ we investigated in the presented study whether this effect could be narrowed down to specific distances by using custom molecular rulers.

As illustrated in Figure 1, the workflow of MOSAIC experiments combines the self-assembly of protein-decorated DON¹¹ and top-down DNA micropatterning²⁹ of glass surfaces. Two different DON designs, a rectangular R-DON ($\sim 91 \times 59 \text{ nm}^2$, Figure 1a) and a narrow longitudinally elongated L-DON ($\sim 185 \times 29 \text{ nm}^2$, Figure 1b), were used as molecular rulers for presentation of EGF ligands to study EGFR activation in adherent cells. The methods for DON assembly and functionalization with biotinylated EGF (bEGF) ligands via streptavidin (STV) bridges were adapted from previous works.^{13,30} As previously shown, EGF retains its binding capabilities for EGFR after being immobilized on a surface.^{31–33} Details of the experimental protocols, origami design, and a full list of oligonucleotide sequences are given in the Supporting Information. In a typical MOSAIC experiment, the DONs were immobilized on a glass surface previously patterned with a DNA microarray containing complementary capture oligonucleotides ($\sim 5 \mu\text{m}$ spot size, 250–500 DONs per spot). Subsequently, the surface was washed to remove unbound DONs. Adherent MCF7 cells stably expressing an eGFP-tagged EGF receptor (eGFP-EGFR) were then allowed to adhere on the micro-/nanopatterned chips for 45 min. After

fixation, activated EGFR was detected by immunostaining using a monoclonal antibody directed against phosphorylated tyrosine residue 1068 of the EGFR ($\alpha\text{P-EGFR-IgG}^{\text{AF647}}$) and a secondary antibody labeled with Alexa Fluor 647 to yield red spots in the fluorescence micrographs (Figure 1d, panel IV). The fluorescent signals shown here originate from micrometer spots, each containing a few hundred origami constructs. It has already been shown that patterning of cell surface receptors on differently patterned substrates has no measurable effect on plasma membrane curvature,^{34–36} indicating a homogeneous cell contact area over the entire cell surface and should also apply to the origami-containing patterns used here.

We note that both MCF7 and HeLa cells are unpolarized cells that do not form distinctive apical and basal membrane. Therefore, it can be assumed that the EGF receptors are initially evenly distributed over the entire cell membrane. Furthermore, we had previously shown that the absence of EGF ligands on the DON constructs leads to no receptor activation and a significantly reduced cellular response, clearly demonstrating that it is not micro-/nanopatterning but the presence of EGF ligands that plays a central role in the initiation of basal EGFR activation and clustering.^{13,18} Because EGF ligands are fixed to the surface via the DON platform and therefore lack lateral mobility, they cannot be pulled along the membrane by EGFR receptors to form clusters with other receptors, as has been shown using EGF immobilized on lipid membranes.³¹ Therefore, our working hypothesis was that the receptors are activated upon binding to the immobilized EGF ligands and that this activation can be relayed through lateral interactions with neighboring unliganded EGFR receptors.³⁷ The extent to which this lateral enhancement is promoted by

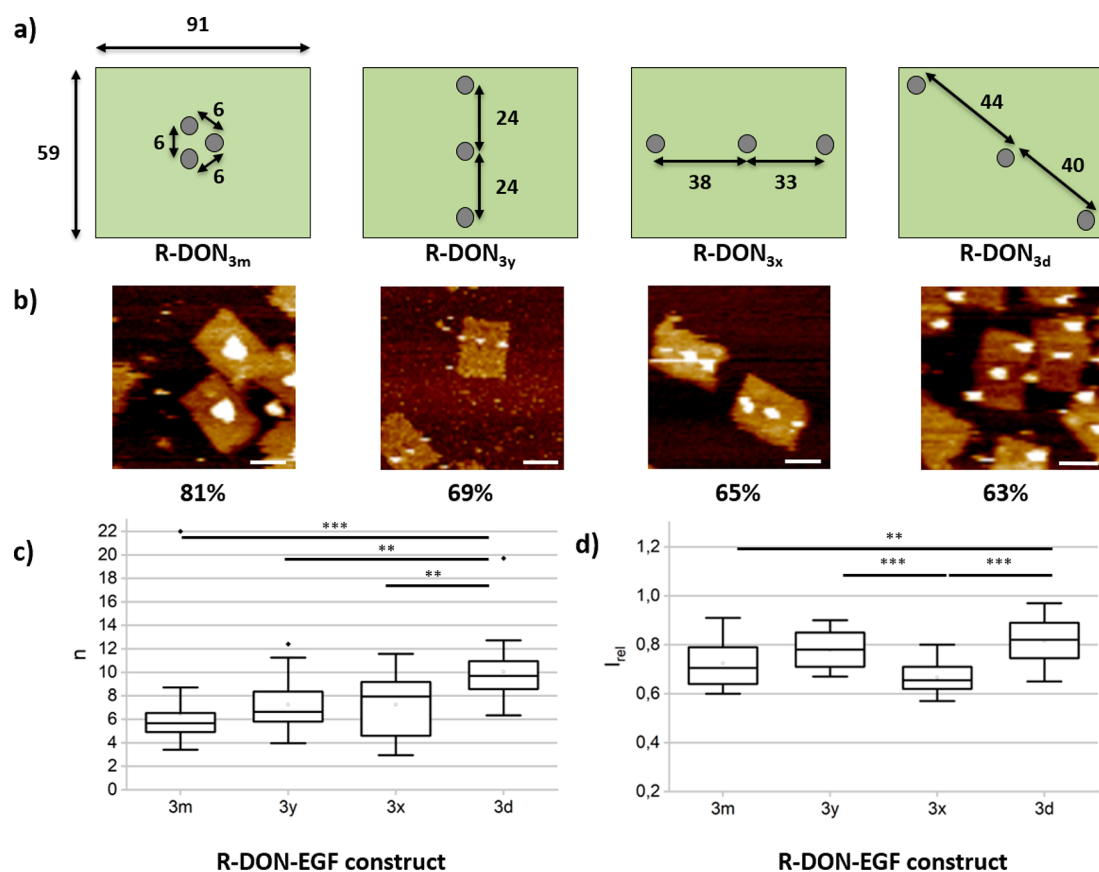


Figure 2. EGFR activation with R-DON rulers presenting three ligand entities arranged in variable distances. (a) Schematic illustration and (b) representative AFM images. The numbers below indicate average surface coverages, determined by AFM (see also Figure S5). Scale bars: 50 nm. (c) Number of activated spots per cell (n) and (d) relative fluorescence intensity (I_{rel}) determined in the activated spots (ratio of red over green channel; see Figure 1) in MOSAIC experiments with eGFP-EGFR-expressing MCF7 cells using the DON constructs shown in (a). For representative fluorescence micrographs, see Figure S6. The box-plot diagrams were generated from the data obtained from the automated image analysis. $**P < 0.01$ and $***P < 0.001$ for comparisons of different spacings using one-way ANOVA followed by Tukey's multiple comparisons test. Only significant differences are indicated. Data were obtained from individual cells ($n \geq 10$) adhered to technical replicate blocks ($n \geq 3$) on a single slide. Each of these analyses was performed for two completely independent biological replicates (on two different days with different batches of R-DON constructs, DNA microarrays, and cells) and used for statistical analysis.

the interligand distances set on the DON should determine the impact on the cellular response.

To quantify the extent to which the structural features of the immobilized EGF-DONs affect EGFR activation in MCF7 cells, statistical analysis was performed to determine the average number of red spots under an adherent cell for the different DON constructs examined. To speed up the statistical analysis of the microarray images, analysis software was developed to automatically count the “activated (red) spots” (Figure S1). In brief, the software processes the Cy3 signal images (indicating successfully hybridized DONs) to determine the spot locations. For each spot, specific features are extracted from the green (origami spots) and red (α P-EGFR-IgG^{AF647}) channel images. Using a self-learning algorithm, a class determination is then applied to recognize the activated (red) spots. Further details and the complete workflow of the software are given in the Supporting Information (Figures S1 and S2, Tables S1–S3). Benchmarking of the software tool by comparing manual and automated analysis of previously collected data¹³ obtained from eight different R-DON constructs containing 4, 5, 8, or 12 EGF ligand units at variable nanometer spacings revealed only minor differences between the manual and automated analysis, indicating that the software tool was working properly (Figure S3).

Reanalysis confirmed that for two DONs with the same number of EGF ligand units but different spacing, the cellular response is significantly enhanced when the ligands are spaced farther apart. This effect was verified in independent multiplex experiments with two differently configured DONs immobilized directly adjacent to each other on the same chip (Figure S4). Because this effect of EGF ligand spacing on cellular response already occurred with only four ligands per DON (Figure S3), the question arose whether even only three EGF ligand units were already sufficient. Because there were always several different spacings in the ligand arrangements investigated so far (Figures S3 and S4a), we also wanted to systematically investigate uniform ligand spacings in the 10–50 nm range because this range seems to play an important role in EGFR activation according to other studies.³⁸

To address these issues, a series of R-DON-based rulers were designed, containing only three ligand units positioned in four different conformations (Figure 2). By arranging ligands in the middle (R-DON_{3m}), along the x - and y -axis (R-DON_{3x} and R-DON_{3y}, respectively) or along the diagonal (R-DON_{3d}) of the rectangular origami scaffold, ligand patterns with almost identical spacings in the range 6–40 nm were realized (Figure 2a). Characterization of these rulers by AFM revealed surface coverages of about 70% (Figures 2b and S5), as is typically

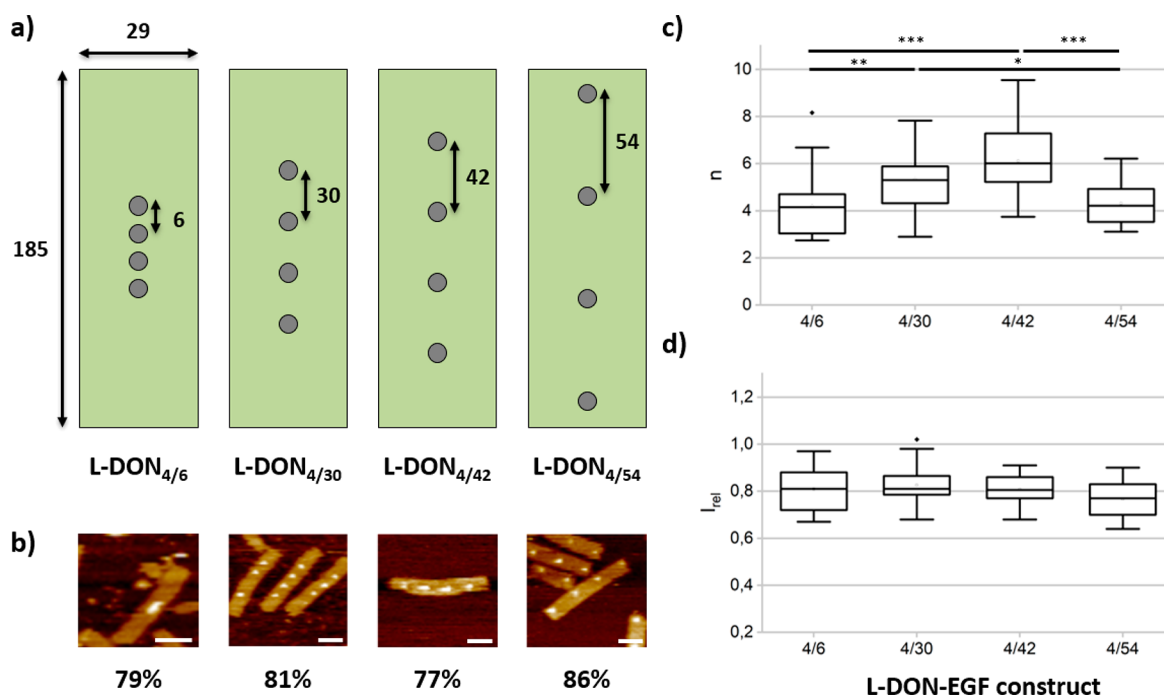


Figure 3. EGFR activation with L-DON rulers presenting linear arrays of four ligands with 6, 30, 42, and 54 nm spacings. (a) Schematic illustration of the rulers and (b) representative AFM images. The numbers below indicate average surface coverages, determined by AFM (see also Figure S8). Scale bars: 50 nm. (c) Number of activated spots per cell (n) and (d) relative fluorescence intensity (I_{rel}) determined in the activated spots (ratio of red over green channel; see Figure 1) in MOSAIC experiments with eGFP-EGFR-expressing MCF7 cells using the DON constructs shown in (a). For representative fluorescence micrographs, see Figure S11. The box-plot diagrams were obtained from the automated image analysis. * $P < 0.05$, ** $P < 0.01$, and *** $P < 0.001$ for comparison of different spacings using one-way ANOVA followed by Tukey's multiple comparisons test. Only significant differences are indicated. Data were obtained from individual cells ($n \geq 10$) adhered to technical replicate blocks ($n \geq 3$) on a single slide. Each of these analyses was performed for two completely independent biological replicates (on two different days with different batches of R-DON constructs, DNA microarrays, and cells) and used for statistical analysis.

observed for this type of protein-decorated DON constructs with standard biotinylated linkers.^{24,39} MOSAIC surfaces were prepared from these constructs as described above and used to stimulate EGFR activation in MCF7 cells (Figure S6 for representative fluorescence micrographs). Data analysis was performed using the software tool described above. Moreover, stability tests were performed to rule out the possibility of degradation due to the presence of DNases in the cell culture medium (Figure S7).

Figure 2c shows that the number of activated spots per cell (n) significantly depended on the immobilized DON construct. A maximal number of active spots was observed for R-DON_{3d} displaying the three EGF entities over a distance of about 40 nm. The ratios between the fluorescence intensities (I_{rel} , Figure 2d) of the positive spots (red channel, indicating the amount of activated EGFR) and the corresponding ones of the green channel (indicating the amount of immobilized R-DON constructs) also suggested that R-DON_{3d} has a higher activation power than the other three arrangements. However, no substantial significance was found in this assay for ligand distances of 6–33 nm. We note that the number of activated spots reflects the extent of cell spreading across the functionalized surface, with intracellular crosstalk between EGFR and integrin receptors^{40,41} likely playing a role. Therefore, the effectors involved in the cellular process that leads to a change in the number of activated sites among cells are likely different from those involved in EGFR phosphorylation alone, which could lead to discrepancies in the observed trends.

Several studies report on EGFR nanocluster formation in unstimulated (~ 150 – 300 nm average cluster size) and EGFR-activated (~ 90 – 150 nm average cluster size) cells, with a significant decrease in cluster size (< 100 nm) and at the same time an increase of the fraction of smaller clusters upon EGFR activation.^{42–44} In order to investigate EGFR activation within the reported nanoscale dimensions using our MOSAIC platform and because the R-DON rulers had the limitation that it is not possible to position a larger number of ligand units with spacings greater than about 40 nm, we designed a novel DON with a narrow, longitudinal shape, in the following termed L-DON (Figure 3a). Four ligand units could be easily positioned with variable interligand spacings on the 185×29 nm² baseplate, resulting in four rulers, L-DON_{4/6}, L-DON_{4/30}, L-DON_{4/42}, and L-DON_{4/54}, with spacings of 6, 30, 42, and 54 nm, respectively. Characterization of the L-DON constructs by AFM revealed higher surface coverages of about 80% (Figures 3b and S7). To check whether the longitudinal base plate lies flat on the solid substrate after DNA-directed immobilization, super-resolution stochastic optical reconstruction microscopy (STORM) measurements were performed (Figure S9). The results clearly showed that the L-DON construct is positioned on the surface in the expected flat, planar conformation. STORM analysis also enabled the precise determination of L-DONs immobilized per spot (481 ± 9) by the applied procedure, which is $\sim 25\%$ higher than that observed for the R-DON constructs (388 ± 9 , Figure S10). Of note, these experimental results confirmed the previously estimated value of 250–500 origami structures per spot, leading to average distances between individual DONs of about 150 nm,¹³ which

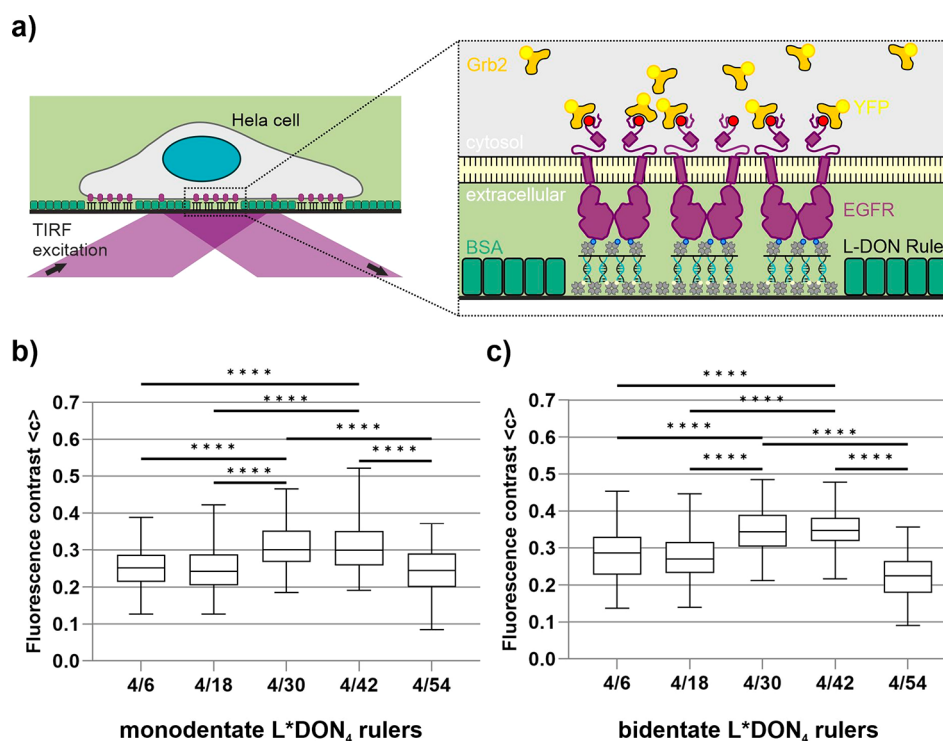


Figure 4. EGFR activation with L*DON₄ rulers presenting linear arrays of four ligands with variable spacings. (a) Schematic representation of TIRF-based analysis of live HeLa cells adherent to MOSAIC spots expressing Grb2-YFP. (b, c) Quantification of Grb2-YFP fluorescence contrast obtained with L*DON₄ rulers decorated with four EGF ligands at variable distances bound via monodentate (b) or bidentate (c) STV bridges. For representative fluorescence micrographs, see Figure S14. Box plots show quantitation of YFP contrast of more than 90 cells measured on at least two different days. **** $P < 0.0001$ for comparison of different spacings using one-way ANOVA followed by Tukey's multiple comparisons test. Only significant differences are indicated.

is significantly larger than the distance between individual ligands on a single DON. We also note that slight changes in surface coverage with DON constructs did not result in significant differences in the activation strength of the respective MOSAIC surfaces.¹³

We then used the L-DON constructs to produce MOSAIC surfaces for the study of EGFR activation in MCF7 cells (for representative fluorescence images, see Figure S11). Figure 3c,d shows the results of the statistical evaluation. It is evident that the number of activated spots per cell (n) increases with increasing distance between ligands up to 42 nm and then drops at a greater distance of 54 nm (Figure 3c). No trend could be derived from the ratio of fluorescence intensities (I_{rel} , Figure 3d) of activated EGFR (red channel) to the amount of immobilized L-DON constructs (green channel), suggesting in combination with the results from Figure 2d that this parameter in the MOSAIC format used may not allow accurate quantification due to insufficient sensitivity between the red and green channels. Nevertheless, the maximum response of cells observed for L-DON constructs with a ligand spacing of about 40 nm correlated very well with the results obtained with the R-DON rulers (Figure 2) and also suggested a decrease in spatial interference at larger ligand spacings.

To further corroborate the results of the MOSAIC system described above, we performed analogue experiments with an alternative platform that differed from the previous system by, first, a commercial scaffold for simplified fabrication of the DON constructs, second, an alternative surface display system, and, third, a different cell line using an alternative biological read-out. The constructs fabricated with the new scaffold, hereafter termed L*DON, allowed attachment of the STV

bridges via both a conventional monodentate biotin linker and bidentate binding through two adjacent biotin groups (Figure S12), resulting in increased stability of protein functionalization.²⁴ Three or four EGF ligand sites were bound per origami, spanning distances between 6–66 and 6–54 nm on L*DON₃ and L*DON₄, respectively, and the resulting constructs were characterized by AFM (Figure S12).

Furthermore, to enable high-throughput in the subcellular micropatterning experiments, we transferred the MOSAIC system to an alternative microarray platform based on multiwell plates.^{18,35} In this method, untreated glass slides were first activated using a polymer metal ion coating and subsequently protein-patterned by large-area microcontact printing with an elastomeric stamp that contained a continuous 3 μm grid pattern to achieve surface passivation with a micrometer-scale BSA grid on the activated glass substrate.³⁴ STV was then immobilized in the resulting unblocked areas, and biotinylated single-stranded DNA capture oligonucleotides were bound to it, thereby enabling attachment of the DON constructs on the glass surface (for the detailed workflow, see Figure S13 and Experimental Procedures). The as-prepared MOSAIC surfaces were incubated with HeLa cells stably expressing the fluorescent fusion protein Grb2-YFP⁴⁵ for at least 3 h and then analyzed by total internal reflection fluorescence microscopy (TIRFM). Grb2 is known to directly bind to phosphorylated tyrosine-containing peptides on receptors (such as EGFR) via its SH2 domain, which results in the activation of downstream kinases.⁴⁶ Therefore, the amount of Grb2 recruited to EGFR can be used as a parameter for EGFR activation by the different DON-patterned surfaces, and thus, the activation efficacy of the different L*DON rulers

can be measured by fluorescence microscopy analysis (Figure 4).

The MOSAIC experiments with L*DON₄ rulers revealed a high degree of specific Grb2 patterning in cells grown on the EGF-decorated DONs, which varied with the specific distances in between the four ligand sites (for representative TIRF microscopy images, see Figure S14). The results obtained with the different L*DON₄ rulers (Figure 4b,c) and showed a high similarity of the distance-dependent activation effect with that obtained with the analogous L-DON₄ rulers (Figure 3). A maximum activation was observed at distances of 30 and 42 nm for both monodentate and bidentate ligand attachment. Compared with the monodentate system, bidentate ligand binding provides increased stability and higher ligand occupancy densities, which is beneficial for recruitment and activation of EGFR²⁴ and explains the slight increase in overall Grb2 co-recruitment.

Further studies performed with a set of L*DON₃ rulers in which three EGF ligand sites were arranged at variable distances between 6 and 66 nm (Figure S15) confirmed the result of the L*DON₄ rulers that distances above 42 nm are not preferred. However, unlike the L*DON₄ rulers, these studies showed that enhanced activation occurs at distances as short as 18 nm. We hypothesize that this could be due to a shift in the oligomerization equilibrium as a result of a variation in EGF density achieved by the same amount of immobilized DON with a different number of ligands per DON. Although it is known that very high EGF concentrations compete with oligomers and lead to the decay of oligomers into smaller units,³⁸ in the present case, EGF density is only slightly increased by ~30% in L*DON₄ compared with L*DON₃. This suggests that we are in the EGF concentration range where increasing EGF dose induces an increase in EGFR aggregation state.^{47,48}

Altogether, the results obtained with the L*DON constructs are remarkable because they correlate very well with that of the L-Ruler constructs although they were generated on an entirely different platform using a different DNA scaffold, solid surface, cells, and biological read-out. The present study is consistent with the consensus in the literature that EGFR is clustered and that clustering plays a role in controlling signal transduction. The characteristic length scale of EGFR clusters was examined in various cell lines by several groups using a variety of microscopy methods.^{42–44,49} Our data can be specifically correlated to a study by Needham et al. in which fluorophore localization imaging with photobleaching was used to study the structure of transiently formed EGFR oligomers, which assemble at physiological EGF concentrations (4 nM).³⁸ The resulting model suggests that interactions of EGFR dimers (diameter ~11 nm) produce oligomers with diameters up to 50–60 nm. Oligomerization organizes kinase-active dimers in a manner optimal for autophosphorylation *in trans* between adjacent dimers, and the appearance of larger oligomers (40 ± 10 nm) was also observed at nonphysiological EGF concentrations.³⁸ These data are in good agreement with the ligand spacing determined by MOSAIC, which led to increased activation and response of the attached cells.

Overall, our work using two different read-out systems, activated spots under a cell (Figures 2 and 3) and fluorescence microscopy-derived recruitment of Grb2 (Figure 4), respectively, demonstrates that varying the nanoscale distance between EGF ligands on the DON surface elicits subtle but statistically significant difference in cellular responses. In light

of the knowledge of the mechanistic mode of action of EGFR activation described above, we hypothesize that the observed differences in cellular responses are related to the degree of correspondence between the nanoscale EGF patterns and the EGFR oligomers resulting from lateral amplification during EGFR activation.³⁷ Our results suggest that under the conditions chosen here, EGFR activation leads mainly to the formation of octa- and decamers spanning 30–40 nm.³⁸ When the surface-bound EGF ligands are presented at this spacing, many such EGFR oligomers can be bound and stabilized, thereby eliciting a stronger cellular response than that with smaller or larger EGF spacings. Longer distances do not seem to be able to maintain lateral activation of these oligomers, leading to their disassembly and a reduced cell response, while conversely shorter distances, such as 18 or 6 nm, can harbor only tetramers or monomers, respectively, while shielding the diffusion of free unbound receptors, leading to the observed decrease in cell response.

In summary, our work illustrates that DNA origami-based surface patterning is a powerful tool to study the influence of nanostructured ligand arrangements on the activation of early cell signaling cascades. The study of cell signaling using artificial surface-based biointerfaces is a common approach that is widely used, even if the artificial environment and immobilization of receptors can potentially affect native cellular conditions, such as dynamic equilibria and thus receptor clustering and cluster size. However, because of the abundant evidence that such microstructured cells retain their native signaling behavior^{7,50–54} and because of the experimental simplicity and high precision for displaying receptor-specific ligands, this approach offers enormous potential for exploring fundamental molecular mechanisms of cell biology. To realize a robust, easily configurable experimental platform for high-throughput MOSAIC assays to investigate receptor activation in adherent cells, the present study specifically addresses technical innovations related to tailored DON constructs and the use of microscopy-based methods for the analysis of micro- and nanostructured surface patterns. Here, the potential for flexible ligand presentation is particularly noteworthy, involving control of stoichiometry and spatial architecture as well as the flexibility of linker systems. We note that the study of cell signaling cascades using DNA-based approaches to ligand presentation on mobile lipid surfaces^{17,55} or as soluble DNA agents^{12,16,22,56} is becoming increasingly popular.⁵⁷ In contrast to these examples, the surface-based MOSAIC approach presented here allows to suppress endocytic desensitization of the stimulated cells and thereby freeze an early stage of cell signaling, for example, to identify the recruitment of downstream signaling components based on specific surface patterns.¹⁸ Thus, the MOSAIC platform has the potential to provide deep insights into complex cell signaling nodes at the plasma membrane without the need for high-resolution imaging techniques, as lateral resolution is already achieved with the DONs and biological response can be measured with “standard” microscopy equipment. We postulate that further refinement of this approach can provide a generic and broadly applicable platform to unravel the complex molecular mechanisms of life.

■ ASSOCIATED CONTENT

Supporting Information

The Supporting Information is available free of charge at <https://pubs.acs.org/doi/10.1021/acs.nanolett.3c04272>.

Experimental procedures and materials, supplemental figures and tables, and an appendix (oligonucleotide sequences) (PDF)

AUTHOR INFORMATION

Corresponding Authors

Christof M. Niemeyer – Institute for Biological Interfaces (IBG-1), Karlsruhe Institute of Technology (KIT), 76344 Eggenstein-Leopoldshafen, Germany; orcid.org/0000-0002-8837-081X; Phone: +49 721 608 23000; Email: niemeyer@kit.edu

Carmen M. Dominguez – Institute for Biological Interfaces (IBG-1), Karlsruhe Institute of Technology (KIT), 76344 Eggenstein-Leopoldshafen, Germany; orcid.org/0000-0002-0918-5473; Email: carmen.dominguez@kit.edu

Authors

Ivy Mayer – Institute for Biological Interfaces (IBG-1), Karlsruhe Institute of Technology (KIT), 76344 Eggenstein-Leopoldshafen, Germany

Tina Karimian – School of Engineering, University of Applied Sciences Upper Austria, 4600 Wels, Austria

Klavdiya Gordiyenko – Institute for Biological Interfaces (IBG-1), Karlsruhe Institute of Technology (KIT), 76344 Eggenstein-Leopoldshafen, Germany

Alessandro Angelin – Institute for Biological Interfaces (IBG-1), Karlsruhe Institute of Technology (KIT), 76344 Eggenstein-Leopoldshafen, Germany

Ravi Kumar – Institute of Nanotechnology (INT) & Karlsruhe Nano Micro Facility (KNMF), Karlsruhe Institute of Technology (KIT), 76344 Eggenstein-Leopoldshafen, Germany

Michael Hirtz – Institute of Nanotechnology (INT) & Karlsruhe Nano Micro Facility (KNMF), Karlsruhe Institute of Technology (KIT), 76344 Eggenstein-Leopoldshafen, Germany; orcid.org/0000-0002-2647-5317

Ralf Mikut – Institute for Automation and Applied Informatics (IAI), Karlsruhe Institute of Technology (KIT), 76344 Eggenstein-Leopoldshafen, Germany

Markus Reischl – Institute for Automation and Applied Informatics (IAI), Karlsruhe Institute of Technology (KIT), 76344 Eggenstein-Leopoldshafen, Germany

Johannes Stegmaier – Institute for Automation and Applied Informatics (IAI), Karlsruhe Institute of Technology (KIT), 76344 Eggenstein-Leopoldshafen, Germany; Institute of Imaging and Computer Vision, RWTH Aachen University, 52074 Aachen, Germany

Lu Zhou – Institute of Applied Physics (APH), Karlsruhe Institute of Technology (KIT), 76049 Karlsruhe, Germany

Rui Ma – Institute of Applied Physics (APH), Karlsruhe Institute of Technology (KIT), 76049 Karlsruhe, Germany

Gerd Ulrich Nienhaus – Institute of Applied Physics (APH), Karlsruhe Institute of Technology (KIT), 76049 Karlsruhe, Germany; Institute of Biological and Chemical Systems (IBCS) and Institute of Nanotechnology (INT), Karlsruhe Institute of Technology (KIT), 76021 Karlsruhe, Germany; Department of Physics, University of Illinois at Urbana-Champaign, Urbana, Illinois 61801, United States; orcid.org/0000-0002-5027-3192

Kersten S. Rabe – Institute for Biological Interfaces (IBG-1), Karlsruhe Institute of Technology (KIT), 76344 Eggenstein-Leopoldshafen, Germany; orcid.org/0000-0001-7909-8191

Peter Lanzerstorfer – School of Engineering, University of Applied Sciences Upper Austria, 4600 Wels, Austria; orcid.org/0000-0003-4512-7964

Complete contact information is available at: <https://pubs.acs.org/10.1021/acs.nanolett.3c04272>

Author Contributions

I.M., T.K., and K.G. contributed equally to this work. I.M. and K.G.: synthesis and characterization of DON, cell experiments on PPL-printed slides. T.K.: cell experiments on microcontact-printed multiwell plates. A.A.: DON design, DON synthesis, and PPL printing. R.K. and M.H.: development of the PPL printing process. R.M., M.R., and J.S.: development of automatic analysis pipeline. L.Z., R.M., and G.U.N.: super-resolution microscopy imaging. K.S.R., P.L., and C.M.D.: data analysis, results discussion, and writing. C.M.N.: supervision, conceptualization, results discussion, and writing. All authors have given approval to the final version of the manuscript.

Notes

The authors declare no competing financial interest.

ACKNOWLEDGMENTS

This work was financially supported in part through GRK 2039 funded by the German Research Foundation (DFG) and through the programs BioInterfaces in Technology and Medicine (BIFTM), Science and Technology of Nanosystems (STN) and Materials Systems Engineering (MSE) of the Helmholtz foundation. We acknowledge experimental help from Ruben Garrecht, Alessa Schipperges, and Simone Weigel in the early phase of the project and support of the Karlsruhe Nano Micro Facility (KNMF, www.knmf.kit.edu), a Helmholtz Research Infrastructure at KIT. T.K. and P.L. acknowledge funding from the “Dissertationsprogramm der Fachhochschule OÖ 2022” with the financial support of the province of Upper Austria (Austrian Research Promotion Agency (FFG) Grant # 895967) and the province of Upper Austria as part of the FH Upper Austria Center of Excellence for Technological Innovation in Medicine (TIMed CENTER).

REFERENCES

- (1) Manz, B. N.; Groves, J. T. Spatial organization and signal transduction at intercellular junctions. *Nat. Rev. Mol. Cell Biol.* **2010**, *11* (5), 342–52.
- (2) Bethani, I.; Skanland, S. S.; Dikic, I.; Acker-Palmer, A. Spatial organization of transmembrane receptor signalling. *EMBO J.* **2010**, *29* (16), 2677–88.
- (3) Hartman, N. C.; Groves, J. T. Signaling clusters in the cell membrane. *Curr. Opin. Cell Biol.* **2011**, *23* (4), 370–6.
- (4) Huang, Y.; Bharill, S.; Karandur, D.; Peterson, S. M.; Marita, M.; Shi, X.; Kaliszewski, M. J.; Smith, A. W.; Isacoff, E. Y.; Kuriyan, J. Molecular basis for multimerization in the activation of the epidermal growth factor receptor. *eLife* **2016**, *5*, No. e14107.
- (5) Ojosnegros, S.; Cutrale, F.; Rodriguez, D.; Otterstrom, J. J.; Chiu, C. L.; Hortiguera, V.; Tarantino, C.; Seriola, A.; Mieruszynski, S.; Martinez, E.; Lakadamyali, M.; Raya, A.; Fraser, S. E. Eph-ephrin signaling modulated by polymerization and condensation of receptors. *Proc. Natl. Acad. Sci. U S A* **2017**, *114* (50), 13188–13193.
- (6) Dustin, M. L.; Groves, J. T. Receptor signaling clusters in the immune synapse. *Annu. Rev. Biophys.* **2012**, *41*, 543–56.
- (7) Torres, A. J.; Wu, M.; Holowka, D.; Baird, B. Nanobiotechnology and cell biology: micro- and nanofabricated surfaces to investigate receptor-mediated signaling. *Annu. Rev. Biophys.* **2008**, *37*, 265–88.

- (8) Schneider, A.-K.; Niemeyer, C. M. DNA Surface Technology: From Gene Sensors to Integrated Systems for Life and Materials Sciences. *Angew. Chem., Int. Ed.* **2018**, *57* (52), 16959–16967.
- (9) Arnold, M.; Cavalcanti-Adam, E. A.; Glass, R.; Blummel, J.; Eck, W.; Kantlehner, M.; Kessler, H.; Spatz, J. P. Activation of integrin function by nanopatterned adhesive interfaces. *ChemPhysChem* **2004**, *5* (3), 383–388.
- (10) Deeg, J. A.; Louban, I.; Aydin, D.; Selhuber-Unkel, C.; Kessler, H.; Spatz, J. P. Impact of Local versus Global Ligand Density on Cellular Adhesion. *Nano Lett.* **2011**, *11* (4), 1469–1476.
- (11) Sacca, B.; Meyer, R.; Erkelenz, M.; Kiko, K.; Arndt, A.; Schroeder, H.; Rabe, K. S.; Niemeyer, C. M. Orthogonal Protein Decoration of DNA Origami. *Angew. Chem., Int. Ed.* **2010**, *49* (49), 9378–9383.
- (12) Shaw, A.; Lundin, V.; Petrova, E.; Fordos, F.; Benson, E.; Al-Amin, A.; Herland, A.; Blokzijl, A.; Hogberg, B.; Teixeira, A. I. Spatial control of membrane receptor function using ligand nanocalipers. *Nat. Methods* **2014**, *11* (8), 841–6.
- (13) Angelin, A.; Weigel, S.; Garrecht, R.; Meyer, R.; Bauer, J.; Kumar, R. K.; Hirtz, M.; Niemeyer, C. M. Multiscale Origami Structures as Interface for Cells. *Angew. Chem., Int. Ed.* **2015**, *54* (52), 15813–15817.
- (14) Huang, D.; Patel, K.; Perez-Garrido, S.; Marshall, J. F.; Palma, M. DNA Origami Nanoarrays for Multivalent Investigations of Cancer Cell Spreading with Nanoscale Spatial Resolution and Single-Molecule Control. *ACS Nano* **2019**, *13* (1), 728–736.
- (15) Hawkes, W.; Huang, D.; Reynolds, P.; Hammond, L.; Ward, M.; Gadegaard, N.; Marshall, J. F.; Iskratsch, T.; Palma, M. Probing the nanoscale organization and multivalency of cell surface receptors: DNA origami nanoarrays for cellular studies with single-molecule control. *Faraday Discuss.* **2019**, *219*, 203–219.
- (16) Veneziano, R.; Moyer, T. J.; Stone, M. B.; Wamhoff, E.-C.; Read, B. J.; Mukherjee, S.; Shepherd, T. R.; Das, J.; Schief, W. R.; Irvine, D. J.; Bathe, M. Role of nanoscale antigen organization on B-cell activation probed using DNA origami. *Nat. Nanotechnol.* **2020**, *15* (8), 716–723.
- (17) Hellmeier, J. P.; Platzer, R.; Karner, A.; Motsch, V.; Bamieh, V.; Preiner, J.; Brameshuber, M. O.; Stockinger, H.; Schütz, G. J.; Huppa, J. B.; Sevcsik, E. Spatial Requirements for T-Cell Receptor Triggering Probed via Functionalized DNA Origami Platforms. *Biophys. J.* **2020**, *118* (3), 245a.
- (18) Lanzerstorfer, P.; Muller, U.; Gordiyenko, K.; Weghuber, J.; Niemeyer, C. M. Highly Modular Protein Micropatterning Sheds Light on the Role of Clathrin-Mediated Endocytosis for the Quantitative Analysis of Protein-Protein Interactions in Live Cells. *Biomolecules* **2020**, *10* (4), 540.
- (19) Hellmeier, J.; Platzer, R.; Eklund, A. S.; Schlichthaerle, T.; Karner, A.; Motsch, V.; Schneider, M. C.; Kurz, E.; Bamieh, V.; Brameshuber, M.; Preiner, J.; Jungmann, R.; Stockinger, H.; Schütz, G. J.; Huppa, J. B.; Sevcsik, E. DNA origami demonstrate the unique stimulatory power of single pMHCs as T cell antigens. *Proc. Natl. Acad. Sci. U. S. A.* **2021**, *118* (4), No. e2016857118.
- (20) Wang, Y.; Baars, I.; Fördös, F.; Högberg, B. Clustering of Death Receptor for Apoptosis Using Nanoscale Patterns of Peptides. *ACS Nano* **2021**, *15* (6), 9614–9626.
- (21) Fang, T.; Alvelid, J.; Spratt, J.; Ambrosetti, E.; Testa, I.; Teixeira, A. I. Spatial Regulation of T-Cell Signaling by Programmed Death-Ligand 1 on Wireframe DNA Origami Flat Sheets. *ACS Nano* **2021**, *15* (2), 3441–3452.
- (22) Berger, R. M. L.; Weck, J. M.; Kempe, S. M.; Hill, O.; Liedl, T.; Radler, J. O.; Monzel, C.; Heuer-Jungemann, A. Nanoscale FasL Organization on DNA Origami to Decipher Apoptosis Signal Activation in Cells. *Small* **2021**, *17* (26), 2101678.
- (23) Cremers, G. A. O.; Rosier, B. J. H. M.; Meijs, A.; Tito, N. B.; van Duijnhoven, S. M. J.; van Eenennaam, H.; Albertazzi, L.; de Greef, T. F. A. Determinants of Ligand-Functionalized DNA Nanostructure–Cell Interactions. *J. Am. Chem. Soc.* **2021**, *143* (27), 10131–10142.
- (24) Domínguez, C. M.; García-Chamé, M.; Müller, U.; Kraus, A.; Gordiyenko, K.; Itani, A.; Haschke, H.; Lanzerstorfer, P.; Rabe, K. S.; Niemeyer, C. M. Linker Engineering of Ligand-Decorated DNA Origami Nanostructures Affects Biological Activity. *Small* **2022**, *18* (35), 2202704.
- (25) Wang, M.; Yang, D.; Lu, Q.; Liu, L.; Cai, Z.; Wang, Y.; Wang, H.-H.; Wang, P.; Nie, Z. Spatially Reprogrammed Receptor Organization to Switch Cell Behavior Using a DNA Origami-Templated Aptamer Nanoarray. *Nano Lett.* **2022**, *22* (21), 8445–8454.
- (26) Frtús, A.; Smolková, B.; Uzhytchak, M.; Lunova, M.; Jirsa, M.; Henry, S. J. W.; Dejneka, A.; Stephanopoulos, N.; Lunov, O. The interactions between DNA nanostructures and cells: A critical overview from a cell biology perspective. *Acta Biomaterialia* **2022**, *146*, 10–22.
- (27) Morzy, D.; Bastings, M. Significance of Receptor Mobility in Multivalent Binding on Lipid Membranes. *Angew. Chem., Int. Ed.* **2022**, *61* (13), No. e202114167.
- (28) Schneider, L.; Rabe, K. S.; Domínguez, C. M.; Niemeyer, C. M. Hapten-Decorated DNA Nanostructures Decipher the Antigen-Mediated Spatial Organization of Antibodies Involved in Mast Cell Activation. *ACS Nano* **2023**, *17* (7), 6719–6730.
- (29) Niemeyer, C. M.; Boldt, L.; Ceyhan, B.; Blohm, D. DNA-Directed Immobilization: Efficient, Reversible and Site-Selective Surface Binding of Proteins by Means of Covalent DNA-Streptavidin Conjugates. *Anal. Biochem.* **1999**, *268*, 54–63.
- (30) Erkelenz, M.; Bauer, D. M.; Meyer, R.; Gatsogiannis, C.; Raunser, S.; Sacca, B.; Niemeyer, C. M. A Facile Method for Preparation of Tailored Scaffolds for DNA-Origami. *Small* **2014**, *10* (1), 73–77.
- (31) Stabley, D.; Retterer, S.; Marshall, S.; Salaita, K. Manipulating the lateral diffusion of surface-anchored EGF demonstrates that receptor clustering modulates phosphorylation levels. *Integr. Biol. (Camb)* **2013**, *5* (4), 659–668.
- (32) Watson, J. L.; Aich, S.; Oller-Salvia, B.; Drabek, A. A.; Blacklow, S. C.; Chin, J.; Derivery, E. High-efficacy subcellular micropatterning of e202009063 using fibrinogen anchors. *J. Cell Biol.* **2021**, *220* (2), No. e202009063.
- (33) Singhai, A.; Wakefield, D. L.; Bryant, K. L.; Hammes, S. R.; Holowka, D.; Baird, B. Spatially Defined EGF Receptor Activation Reveals an F-Actin-Dependent Phospho-Erk Signaling Complex. *Biophys. J.* **2014**, *107* (11), 2639–2651.
- (34) Karimian, T.; Hager, R.; Karner, A.; Weghuber, J.; Lanzerstorfer, P. A Simplified and Robust Activation Procedure of Glass Surfaces for Printing Proteins and Subcellular Micropatterning Experiments. *Biosensors* **2022**, *12* (3), 140.
- (35) Hager, R.; Müller, U.; Ollinger, N.; Weghuber, J.; Lanzerstorfer, P. Subcellular Dynamic Immunopatterning of Cytosolic Protein Complexes on Microstructured Polymer Substrates. *ACS Sens* **2021**, *6* (11), 4076–4088.
- (36) Dirscherl, C.; Löchte, S.; Hein, Z.; Kopicki, J.-D.; Harders, A. R.; Linden, N.; Karner, A.; Preiner, J.; Weghuber, J.; Garcia-Alai, M.; Uetrecht, C.; Zacharias, M.; Piehler, J.; Lanzerstorfer, P.; Springer, S. Dissociation of β 2m from MHC class I triggers formation of noncovalent transient heavy chain dimers. *J. Cell Sci.* **2022**, *135* (9), jcs259489.
- (37) Ichinose, J.; Murata, M.; Yanagida, T.; Sako, Y. EGF signalling amplification induced by dynamic clustering of EGFR. *Biochem. Biophys. Res. Commun.* **2004**, *324* (3), 1143–1149.
- (38) Needham, S. R.; Roberts, S. K.; Arkhipov, A.; Mysore, V. P.; Tynan, C. J.; Zanetti-Domingues, L. C.; Kim, E. T.; Losasso, V.; Korovesis, D.; Hirsch, M.; Rolfe, D. J.; Clarke, D. T.; Winn, M. D.; Lajevardipour, A.; Clayton, A. H. A.; Pike, L. J.; Perani, M.; Parker, P. J.; Shan, Y.; Shaw, D. E.; Martin-Fernandez, M. L. EGFR oligomerization organizes kinase-active dimers into competent signalling platforms. *Nat. Commun.* **2016**, *7*, 13307.
- (39) Niemeyer, C. M. Semisynthetic DNA-Protein Conjugates for Biosensing and Nanofabrication. *Angew. Chem., Int. Ed.* **2010**, *49* (7), 1200–1216.

- (40) Shahal, T.; Geiger, B.; Dunlop, I. E.; Spatz, J. P. Regulation of Integrin Adhesions by Varying the Density of Substrate-Bound Epidermal Growth Factor. *Biointerphases* **2012**, *7* (1), 23.
- (41) Rao, T. C.; Ma, V. P.-Y.; Blanchard, A.; Urner, T. M.; Grandhi, S.; Salaita, K.; Mattheyses, A. L. EGFR activation attenuates the mechanical threshold for integrin tension and focal adhesion formation. *J. Cell Sci.* **2020**, *133* (13), jcs238840.
- (42) Abulrob, A.; Lu, Z.; Baumann, E.; Vobornik, D.; Taylor, R.; Stanimirovic, D.; Johnston, L. J. Nanoscale imaging of epidermal growth factor receptor clustering: effects of inhibitors. *J. Biol. Chem.* **2010**, *285* (5), 3145–56.
- (43) Zhang, S.; Reinhard, B. M. Characterizing Large-Scale Receptor Clustering on the Single Cell Level: A Comparative Plasmon Coupling and Fluorescence Superresolution Microscopy Study. *J. Phys. Chem. B* **2019**, *123* (26), 5494–5505.
- (44) Wang, Y.; Gao, J.; Guo, X.; Tong, T.; Shi, X.; Li, L.; Qi, M.; Wang, Y.; Cai, M.; Jiang, J.; Xu, C.; Ji, H.; Wang, H. Regulation of EGFR nanocluster formation by ionic protein-lipid interaction. *Cell Res.* **2014**, *24* (8), 959–976.
- (45) Lanzerstorfer, P.; Borgmann, D.; Schütz, G.; Winkler, S. M.; Höglinger, O.; Weghuber, J. Quantification and Kinetic Analysis of Grb2-EGFR Interaction on Micro-Patterned Surfaces for the Characterization of EGFR-Modulating Substances. *PLoS One* **2014**, *9* (3), No. e92151.
- (46) Kozer, N.; Barua, D.; Henderson, C.; Nice, E. C.; Burgess, A. W.; Hlavacek, W. S.; Clayton, A. H. A. Recruitment of the Adaptor Protein Grb2 to EGFR Tetramers. *Biochemistry* **2014**, *53* (16), 2594–2604.
- (47) Kozer, N.; Barua, D.; Orchard, S.; Nice, E. C.; Burgess, A. W.; Hlavacek, W. S.; Clayton, A. H. A. Exploring higher-order EGFR oligomerisation and phosphorylation—a combined experimental and theoretical approach. *Mol. BioSyst.* **2013**, *9* (7), 1849–1863.
- (48) Wollman, A. J. M.; Fournier, C.; Llorente-Garcia, I.; Harriman, O.; Payne-Dwyer, A. L.; Shashkova, S.; Zhou, P.; Liu, T.-C.; Ouaret, D.; Wilding, J.; Kusumi, A.; Bodmer, W.; Leake, M. C. Critical roles for EGFR and EGFR–HER2 clusters in EGF binding of SW620 human carcinoma cells. *J. R. Soc. Interface.* **2022**, *19* (190), 20220088.
- (49) Xu, H.; Zhang, J.; Zhou, Y.; Zhao, G.; Cai, M.; Gao, J.; Shao, L.; Shi, Y.; Li, H.; Ji, H.; Zhao, Y.; Wang, H. Mechanistic Insights into Membrane Protein Clustering Revealed by Visualizing EGFR Secretion. *AAAS Research* **2022**, 2022, 9835035.
- (50) Spatz, J. P.; Geiger, B. Molecular engineering of cellular environments: cell adhesion to nano-digital surfaces. *Methods Cell Biol.* **2007**, *83*, 89–111.
- (51) Satav, T.; Huskens, J.; Jonkheijm, P. Effects of Variations in Ligand Density on Cell Signaling. *Small* **2015**, *11* (39), 5184–99.
- (52) Schwarzenbacher, M.; Kaltenbrunner, M.; Brameshuber, M.; Hesch, C.; Paster, W.; Weghuber, J.; Heise, B.; Sonnleitner, A.; Stockinger, H.; Schutz, G. J. Micropatterning for quantitative analysis of protein-protein interactions in living cells. *Nat. Methods* **2008**, *5* (12), 1053–60.
- (53) Nair, P. M.; Salaita, K.; Petit, R. S.; Groves, J. T. Using patterned supported lipid membranes to investigate the role of receptor organization in intercellular signaling. *Nat. Protoc.* **2011**, *6* (4), 523–39.
- (54) Gandor, S.; Reisewitz, S.; Venkatachalapathy, M.; Arrabito, G.; Reibner, M.; Schroder, H.; Ruf, K.; Niemeyer, C. M.; Bastiaens, P. L.; Dehmelt, L. A Protein-Interaction Array Inside a Living Cell. *Angew. Chem., Int. Ed.* **2013**, *52*, 4890–4894.
- (55) Taylor, M. J.; Husain, K.; Gartner, Z. J.; Mayor, S.; Vale, R. D. A DNA-Based T Cell Receptor Reveals a Role for Receptor Clustering in Ligand Discrimination. *Cell* **2017**, *169* (1), 108–119.e20.
- (56) Sil, D.; Lee, J. B.; Luo, D.; Holowka, D.; Baird, B. Trivalent ligands with rigid DNA spacers reveal structural requirements for IgE receptor signaling in RBL mast cells. *ACS Chem. Biol.* **2007**, *2* (10), 674–84.
- (57) Yeldell, S. B.; Seitz, O. Nucleic acid constructs for the interrogation of multivalent protein interactions. *Chem. Soc. Rev.* **2020**, *49* (19), 6848–6865.